

03,12

## Determination of 2DEG parameters in LED heterostructures with three quantum wells $\text{In}_x\text{Ga}_{1-x}\text{N}/\text{GaN}$ by terahertz time-domain spectroscopy (THz-TDs)

© E.R. Burmistrov, L.P. Avakyants

Moscow State University,  
Moscow, Russia

E-mail: eugeni.conovaloff@yandex.ru

Received October 19, 2022

Revised November 5, 2022

Accepted November 6, 2022

Terahertz time-domain spectroscopy (THz-TDs) has been used to record the resonant frequencies of plasmon oscillations excited in samples of heterostructures with three  $\text{In}_x\text{Ga}_{1-x}\text{N}/\text{GaN}$  quantum wells (QWs) by laser pulses with a duration of 130 fs in the temperature range from 90 to 170 K. Fast Fourier transform (FFT) of the time dependence of the electric field of THz-pulses made it possible to obtain the frequency spectra of the power and phase shift of THz-radiation, the interpretation of which made it possible to estimate the pulse relaxation time, mobility and effective mass of two-dimensional electron gas (2DEG) in the heterostructures. Using a series of frequency spectra of the power and phase shift of THz-radiation, the temperature dependences of the effective mass and relaxation time of the 2DEG pulse were obtained. Mobility value 2DEG obtained by the THz-TDs is in good agreement with the data of Hall measurements.

**Keywords:** heterostructures, pulse relaxation time, 2DEG, terahertz radiation, terahertz spectroscopy.

DOI: 10.21883/PSS.2023.02.55399.503

### 1. Introduction

The method of terahertz time-domain spectroscopy (THz-TDs) is based on generation of terahertz pulses and detection of their waveforms by optical pulses of femto-second duration [1]. The direct measurement of terahertz pulse waveforms allows obtaining information on phase shift of the terahertz radiation, meaning it opens the possibility to investigate mechanisms of relaxation mechanisms involving charge carriers.

The THz-TDs method has shown its efficiency in investigations of systems at low temperatures (5–10 K) temperatures and with low ( $10^{11}$ – $10^{13}$  cm<sup>-3</sup>) electron density, such as, for example, discharge helium (He) plasma [2,3]. In [4,5] the THz-TDs method was used to investigate conductivity, mobility and density of charge carriers in  $\text{CuInSe}_2$  polycrystals and in  $\text{Ge}_2\text{Sb}_2\text{Te}_5$  semiconductor compounds at 7 K. In combination with the density functional theory the THz-TDs method was used to study conductive properties of topological insulators and superconductors [6]. Thus, the THz-TDs completes widely used methods of IR-spectroscopy, Raman scattering and expands the frequency range under study.

In the process of terahertz radiation generation in  $\text{In}_x\text{Ga}_{1-x}\text{N}/\text{GaN}$  heterostructures with multiple quantum wells (MQW), the authors of [7] have found (simultaneously with the photoluminescence) a dependence between the output power of the terahertz radiation and the number of QWs in the active region. According to the results reported in [7], an increase in number of QWs and concentration of

In the GaN barrier leads to an increase in amplification of the terahertz radiation output power.

In [8] the authors investigated experimentally the terahertz radiation generation by laser pulses with a duration of 35 fs at a wavelength of 800 nm in nitride-gallium heterostructures. The authors relate the radiation of terahertz waves with the two-photon absorption of optical laser pulses in MQW. Also, in [8] it is shown that with addition of a QW into the active region of a heterostructure an increase in terahertz radiation amplitude and a shift of its maximum towards the short-wave region is observed. In combination with photoexcitation, the THz-TDs method is used to determine type of conductivity, diffusion length of electrons and holes, and dynamics of radiative recombination in heterostructures [9–11].

Advantages of the THz-TDs method for the studying of semiconductor structures are that the terahertz frequency range contains the information on features of 2DEG dynamics in MQW. In the case of heterostructures these features can be the mobility, the relaxation time of 2DEG, as well as the conductivity.

$\text{InGaN}/\text{AlGaIn}/\text{GaN}$  heterostructures with built-in piezoelectric fields are used as sources of the terahertz radiation. The power of terahertz radiation generated with the help of  $\text{InGaN}/\text{AlGaIn}/\text{GaN}$  heterostructures is proportional to the strength of built-in field, which can be as high as 3 MV/cm [12,8]. Thus,  $\text{InGaN}/\text{AlGaIn}/\text{GaN}$  heterostructures transform ultrashort optical pulses into terahertz electromagnetic waves [13]. Studying of conductive properties of  $\text{InGaN}/\text{AlGaIn}/\text{GaN}$  heterostructures is an actual task due

to their wide practical applications [14,15]. For example, UV-light emitting diodes based on InGaN/AlGaIn/GaN heterostructures have a radiation efficiency of 40% [16–18]. However, output power and radiation efficiency of micro- and opto-electronic devices based on InGaN/AlGaIn/GaN heterostructures are defined by the mobility of 2DEG in In<sub>x</sub>Ga<sub>1-x</sub>N/GaN MQWs. The goal of this study is to determine by the THz-TDs method the pulse relaxation time, mobility, and effective mass of 2DEG in In<sub>x</sub>Ga<sub>1-x</sub>N/GaN heterostructures with three QWs, which are currently widely used in light emitting diodes of blue and green radiation range. Due to the difficulties in interpretation of experimental spectra, there are not much reports on them. In this study we use the previously suggested algorithm to process waveforms of terahertz pulses, which is aimed at numerical evaluation of 2DEG parameters [19].

## 2. Experimental samples

The subject of this study is a layer structure, which is typical for light-emitting diode In<sub>x</sub>Ga<sub>1-x</sub>N/GaN heterostructures with three quantum wells in the active region (Fig. 1). We have investigated industrial samples available samples of InGaIn/AlGaIn/GaN heterostructures grown by the method of vapor-phase epitaxy (VPE).

For InGaIn/AlGaIn/GaN heterostructures on a Al<sub>2</sub>O<sub>3</sub> substrate with an area of 0.4 mm<sup>2</sup> and a thickness of 430 μm, in the [0001] direction the first grown layer was a seed low-temperature layer of GaN with a thickness of 5 μm intended to decrease the mismatching in lattice constants between the layers to be formed. To improve structural quality of the semiconductor and to reduce the density of dislocations, a buffer smoothing superlattice of InGaIn/GaN (20 periods of QWs/QBs with thicknesses of 2/2 nm) was formed in layers of the heterostructure. The active region of the In<sub>x</sub>Ga<sub>1-x</sub>N/GaN heterostructure is composed of three QWs/QBs with thicknesses of 2.5/15 nm. A layer of AlGaIn with a thickness of 20 nm and a layer of GaN with a thickness of 110 nm were formed. The bandgap (equal to  $E_g = 2.6$  eV) and the molar fraction of Indium ( $x_{In} = 0.22$ ) were determined using the method of photocurrent spectroscopy (PCS), as it is described, for example, in [20,21]. The main parameters of the studied samples are given in Table 1.

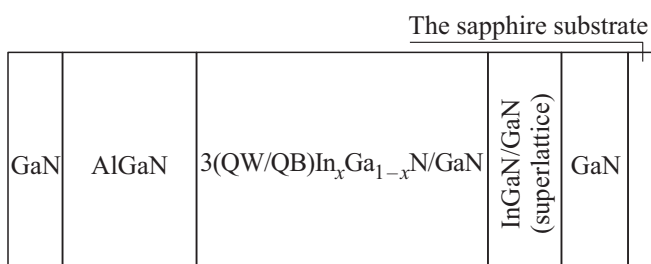


**Figure 1.** Layer structure of the investigated sample.

**Table 1.** Parameters of a heterostructure sample with three In<sub>x</sub>Ga<sub>1-x</sub>N/GaN QWs

Number of QWs, $N$	QW/QB, nm	Surface area of the crystal, mm <sup>2</sup>	$x_{In}$	$E_g$ , eV
3	2.5/15	0.4	0.22	2.6

The serial production of finished light emitting diode devices based on MQWs of In<sub>x</sub>Ga<sub>1-x</sub>N/GaN uses the growth along the polar direction [0001] of the hexagonal GaN. As a result of piezoelectric and spontaneous polarizations, piezoelectric fields with a strength of the order of magnitude of units of MV/cm are formed in the active region of InGaIn/AlGaIn/GaN heterostructures. Usually, to evaluate the strength of piezoelectric field, the dependence of the transition energy between ground (non-excited) levels in QWs of valence band and conduction band on the external electric field is investigated. This approach is based on the quantum-confined Stark effect (QCSE) [20].

Based on the results obtained by the method of photocurrent spectroscopy (PCS), as well as on the results of [22], it can be assumed that:

1. The distribution of built-in electric fields in InGaIn/AlGaIn/GaN heterostructures under study is homogeneous.
2. Deformation shears in the active layer of InGaIn/AlGaIn/GaN heterostructures can be neglected. The power of output terahertz radiation measured by a Golay cell was 3 μW. Hence, the sample under study corresponds to the transmission region of terahertz radiation and the conversion of femtosecond pulse power into the terahertz radiation power is 0.005%.

## 3. Experimental methodology

In this study we have proposed a technique to record frequency spectra of power and phase shift of terahertz radiation, which is based on the excitation of plasmon oscillations by femtosecond optical pulses in In<sub>x</sub>Ga<sub>1-x</sub>N/GaN heterostructures with three QWs. All measurements were carried out on the setup, the scheme of which is shown in Fig. 2

In the investigated InGaIn/AlGaIn/ GaN heterostructures, the Fermi level of the surface state is different from the volumetric Fermi level. Hence, the bandgap boundary becomes curved near the surface. In the region of curvature built-in electric fields are formed, which result in a redistribution of electron density deep into the semiconductor. As a result of multiphoton absorption of femtosecond laser pulses in QWs of InGaIn space-separated electrons and holes appear. Under the action of the built-in piezoelectric field the electron-hole pair becomes polarized [23]. This leads to generation of a time-varying dipole moment  $P(t)$  in the

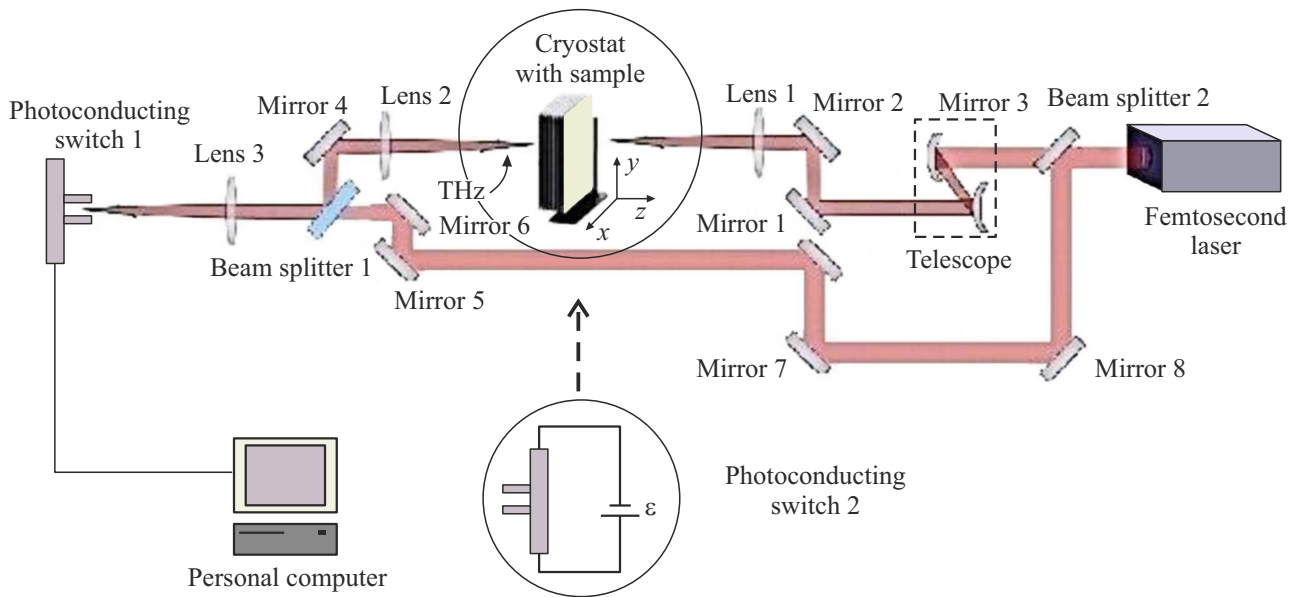


**Figure 2.** Diagram of the experimental setup used to generate terahertz pulses and detect their waveforms.

system, which in turn leads to the radiation of terahertz electromagnetic waves.

In the scheme (Fig. 2) the source of radiation is a Ti: sapphire laser with a pulse time window of  $T_1 = 130$  fs at a wavelength of 800 nm, with a mean output radiation power of 57 mW and with a pulse repetition rate of 60 MHz. The optical and terahertz radiation paths were pre-adjusted. Waveforms of terahertz pulses were recorded in the transmission geometry. The radiation of Ti: sapphire laser with a beam diameter of 1.8 mm was separated into a pump beam and a probe beam (reference) (Fig. 2). Since the size of IR-radiation spot on the heterostructure surface was greater than the IR-radiation wavelength, it was necessary to take into account the interference from elementary sources in the cross-section of the spot, that caused modulation of the resulted pattern. The maximum power of terahertz radiation generation is observed in the case when oscillations of elementary sources are added in-phase along the direction of elementary dipole radiation, i.e. along the tangent line to the heterostructure surface. Therefore the pump beam with  $P$ -polarization of electric field fell at the Brewster angle on the heterostructure surface (Fig. 3). When falling at the Brewster angle, the IR-radiation with  $P$ -polarization of electric field is transmitted with maximum efficiency through the sample without reflection. At the output from the sample the divergent terahertz radiation was focused by a silicone lens 2, a mirror 4 and was directed to a detector. The reference was used to control the detector, which was sensitive to the electric field of terahertz pulses.

To separate the dipole response of 2DEG from oscillations of different physical nature arising as a result of terahertz pulses generation in InGaN/AlGaIn/GaN heterostructures, the terahertz pulses were time gated. For the purpose

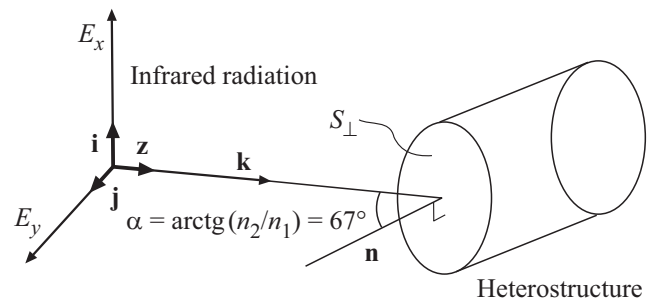


**Figure 3.** Scheme of the experiment geometry, where  $n_1$  — refractive index of the medium from which the IR-radiation falls on the heterostructure surface,  $n_2$  — refractive index of GaN,  $\alpha$  — Brewster angle for the InGaN/AlGaIn/GaN heterostructure,  $\mathbf{k}$  — wave vector of IR-radiation,  $\mathbf{n}$  — normal to the surface.

of selective pickup of time sections of the terahertz pulses and recording of time dependence of their electric field, time windows (or gates) were used. The larger is the time window, the higher frequencies can be detected. Changing the time delay between the reference and the pump pulse allowed selecting the time window width [24]. In the time window pulses were recorded that corresponded to the dipole response of 2DEG and other pulses were suppressed. When the time windows were used, the pulse response of the substance was multiplied by a window function. In the frequency domain it corresponds to convolution of the pulse response to window spectrum. The terahertz and optical pulses (the pump pulse and the reference) are replicas of the same femtosecond pulse. Hence, the terahertz pulse and the reference are connected to each other by phase and this connection remains unchanged over time. Length of the pump pulse (130 fs) is less than the period of terahertz

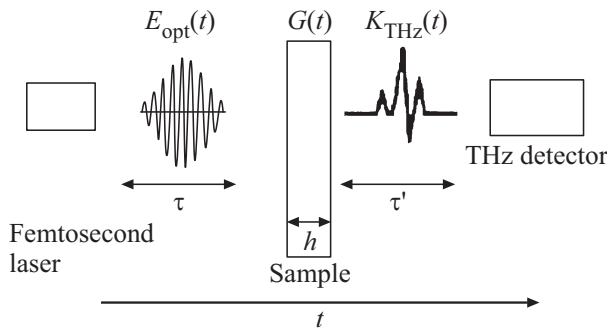


**Figure 4.** Scheme illustrating the mechanism of formation of plasmon oscillations excited in MQW of  $\text{In}_x\text{Ga}_{1-x}\text{N}/\text{GaN}$ . A time scale is shown that indicates the direction of propagation of the optical and terahertz pulses.

pulse. Hence, the reference interacts on the detector with the same time section of the terahertz pulse. The detector was gated in the time domain using an optical system of delay composed of mirrors 7, 8 with adjustable distance between them. By varying the distance between mirrors 7 and 8, the time of reference arrival to the detector was adjusted in relation to the terahertz pulse. This allowed detecting different sections of the terahertz pulse with a time resolution equal to the length of the reference. Step of the displacement was 17 fs ( $5\ \mu\text{m}$ ).

Terahertz pulses were detected using a photoconductive antenna (PC1). It is made up of two metal electrodes located on a semiconductor isolating substrate with a working surface of  $30 \times 40\ \mu\text{m}$  made of low-temperature GaAs with a thickness of  $3\ \mu\text{m}$ , grown by the VPE method at a temperature of  $300^\circ\text{C}$ . Electrodes of the PC1 were connected to a current meter. The electric current proportional to the amplitude of electric field of terahertz pulses was created by photoexcited charge carriers moving in the electric field

$$J = \langle N \rangle e \mu E(\tau), \quad (1)$$

where  $\langle N \rangle$  — mean value of photoexcited carriers concentration, adjustable time delay of the reference in relation to the pump pulse. The electric field of terahertz pulses was recorded in different time intervals, which allowed carrying out measurements at required moments of time. The Fourier transform was used for the transition from time domain to frequency domain. The terahertz emission spectra were visualized and processed by means of a personal computer.

Let the electric field of a femtosecond pulse with a duration of  $\tau$  is described by  $E_{\text{opt}}(t)$  function, while its intensity is described by  $I_{\text{opt}}(t)$  function (Fig. 4).

Let  $G(t)$  function characterizes the phase modulation of the terahertz radiation due to its passage through a sample with a thickness of  $h$ . Then, the signal on detector  $N(t')$  can be represented in the form of convolution of two functions, one of which  $K_{\text{THz}}(t)$  corresponds to the electric field of

terahertz pulses

$$N(t') = I_{\text{opt}}(t) \otimes K_{\text{THz}}(t'). \quad (2)$$

Phase modulation caused by the time delay of the terahertz pulse in the sample can be taken into account integrally by linking the  $K_{\text{THz}}(t)$  with the function of electric field of the IR-radiation

$$K_{\text{THz}}(t) = \int_{-\infty}^{+\infty} G(t-t') E_{\text{opt}}(t') dt'. \quad (3)$$

The fast Fourier transform was used for the transition from time domain to frequency domain. In this case the convolution of functions is represented as a product of Fourier transforms:

$$K_{\text{THz}}(\omega) = G(\omega) E_{\text{opt}}(\omega). \quad (4)$$

In equation (4)  $G(\omega)$  is a complex-valued function of modulation transfer. The physical meaning that corresponds to the modulation of monochromatic radiation is possessed by  $\text{Re}[G(\omega)]$ . In the THz-TDs method the resulted spectrum is a superposition of Fourier transforms of a terahertz and a weak optical pulse

$$G(\omega) = \frac{\frac{1}{\sqrt{2\pi}} \int_{-\infty}^{+\infty} K_{\text{THz}}(t) \exp(-i\omega t) dt}{\frac{1}{\sqrt{2\pi}} \int_{-\infty}^{+\infty} E_{\text{opt}}(t) \exp(-i\omega t) dt} = \frac{K_{\text{THz}}(\omega)}{E_{\text{opt}}(\omega)}. \quad (5)$$

Time shift of two terahertz pulses in relation one to another by  $\Delta t$  due to the finite time of 2DEG reconfiguration in MQW results in a phase shift of one of them, which can be taken into account as follows:

$$K_{\text{THz}}(\omega) \exp(-i\omega \Delta t) = \int_{-\infty}^{+\infty} K_{\text{THz}}(t - \Delta t) \exp(-i\omega t) dt. \quad (6)$$

As was already mentioned above, length of the optical pulse is less than that of the terahertz pulse. Hence, the  $I_{\text{opt}}(t)$  function can be approximated using the delta-function  $\delta(t)$ . Equation (2) takes the following form

$$\begin{aligned} N(t') &= I_{\text{opt}}(t) \otimes K_{\text{THz}}(t') \approx \delta(t) \otimes K_{\text{THz}}(t') \\ &= K_{\text{THz}}(t'). \end{aligned} \quad (7)$$

The latter means that a waveform of the terahertz pulse can only be recorded, when it simultaneously interacts with the reference on the detector. Hence, the THz-TDs method can record phase shift, power, and electric field of terahertz pulses as functions of time.

We recorded two waveforms of electric field of terahertz pulses:  $E_{\text{on}}(t)$  and  $E_{\text{off}}(t)$ . The  $E_{\text{on}}(t)$  waveform of the terahertz pulse passed through the heterostructure was detected in accordance with the diagram shown in Fig. 2. To record

the  $E_{\text{off}}(t)$  time dependence we used two photoconductive antennas. One of them (PC1) was used as a detector of terahertz pulses. Another (PC2) was located instead of the cryostat with samples and used to transform the incoming femtosecond pulses to terahertz pulses (Fig. 2). Electrodes of the PC2 were connected to the power supply source. The terahertz pulses generated on the PC2 were fed to the PC1. The  $E_{\text{off}}(t)$  time dependence was recorded using the reference, which time of arrival was regulated by the optical delay system.

The transition from time representation of terahertz pulse waveforms to frequency representation of them was implemented through the use of fast Fourier transform (FFT) mechanism. This allowed us to expand waveforms of terahertz pulses into individual Fourier-harmonics [24]:

$$E_{\text{off,on}}(f) = |E_{\text{off,on}}(f)| \exp(\varphi_{\text{off,on}}(f)). \quad (8)$$

FFT of the  $E_{\text{on}}(t)$  time dependence allowed identifying the minima that correspond to resonance frequencies of 2D plasmon oscillations.

To characterize terahertz emission spectra we evaluated such parameters as spectral power  $P_i(f) = |E_{\text{on}}(f)|^2 / |E_{\text{off}}(f)|^2$  and phase shift  $\Phi_i(f) = \varphi_{\text{on}}(f) - \varphi_{\text{off}}(f)$ . The phase unwrapping method was applied to determine the  $\Phi_i(f)$  total phase, which corresponds to the number of transitions fitting within the path difference of wavelengths of the radiation falling and passing through the cryostat with samples. For this purpose  $2\pi$  multiplier was added to each phase value within the first period. It was pre-defined that there were no phase steps in the points of passing over the period. The path difference of wavelengths was determined in the process of the experiment.

To smooth and model the time dependence of  $E_{\text{on}}(f)$ , an expansion into the Fourier series was performed with Fourier-components of the time dependence of  $E_{\text{off}}(f)$  calculated by formula (8) and with complex transfer function  $F(f)$ :

$$E_{\text{sim}}(f) = F(0)E_{\text{off}}(0) + \sum_k F(f_k)E_{\text{off}}(f_k) \exp(2\pi i f_k t), \quad (9)$$

where  $F(f)$  was determined by solving the Maxwell equations in a hydrodynamic model of high-frequency properties of the 2DEG as a response of the medium to a plane wave with a frequency of  $f$ ,  $k_K = k/\Delta t$ ,  $k = 1, 2, \dots$  and  $\Delta t$  being the time window of pulses. The  $F(f_k)$  function depends on the dielectric environment of the 2DEG. When determining function  $F(t)$ , the GaN barrier layer and the substrate were modeled as two different layers with complex dielectric permittivities  $\varepsilon_d$  and  $\varepsilon_s$ . The expressions for  $\varepsilon_d$  and  $\varepsilon_s$  took into account the components  $\text{Im}[\varepsilon_d]$  and  $\text{Im}[\varepsilon_s]$ , which are responsible for energy losses in plane-parallel layers of the heterostructure.

For the plasmon structures under consideration the resonance frequencies were evaluated from the dispersion

law of the gated 2D plasmons [25,26]:

$$f_{g,n} = \frac{1}{2\pi} \sqrt{\frac{4\pi e^2 N_{2\text{DEG}} |q_n|}{m^* \varepsilon_0 (\varepsilon_s + \varepsilon_d \coth(|q_n| d_{2\text{DEG}}))}}, \quad (10)$$

where  $q_n = 2\pi n/P$ ,  $n = 1, 2, \dots$  ( $n = 3$  in the case of  $\text{In}_x\text{Ga}_{1-x}\text{N}/\text{GaN}$  heterostructures with three QWs),  $P$  — period of the active region composed of three QWs of  $\text{In}_x\text{Ga}_{1-x}\text{N}/\text{GaN}$  ( $P = 17.5$  nm),  $\varepsilon_s = 10.6 + i\alpha$  — dielectric permittivity of the substrate,  $\varepsilon_d = 9.5 + i\beta$  — dielectric permittivity of the barrier,  $m^*$  — effective mass determined from (10),  $\varepsilon_0$  — dielectric constant,  $d_{2\text{DEG}}$  — depth of 2DEG occurrence in the  $\text{InGaN}/\text{AlGaIn}/\text{GaN}$  heterostructure ( $d_{2\text{DEG}} = 36$  nm). In the imaginary parts of complex dielectric permittivities we have introduced fitting parameters  $\alpha = 20.7$ ,  $\beta = 131.3$ , which allowed us to take into account radiation losses in the substrate and in the region of barriers of the heterostructure's active layer. Values of the fitting parameters were selected to achieve the best matching between the modelled signal  $E_{\text{sim}}(t)$  and the measurement data in the process of determining the  $F(f)$  function. For the spectral range below the first plasmon resonance frequency, i.e.  $f < f_{g,11.6}$ , it was taken into account that  $\varepsilon_s$  and  $\varepsilon_d$  are dispersionless parameters with constant values of 11.6 and 10.5, respectively. The substitution of resonance frequencies to formula (10) allowed for evaluation of the effective mass  $m^*$ . Based on the pulse relaxation times  $\tau$  and effective mass, we determined mobility ( $\mu = e\tau/m^*$ ) of 2DEG in three QWs of  $\text{In}_x\text{Ga}_{1-x}\text{N}/\text{GaN}$ .

Hall mobility and concentration for the heterostructures under study were determined in the geometry of Van der Pauw. Temperature dependences of Hall concentration and mobility were recorded using a „Ecopia HMS-3000“ unit in magnet fields of up to 6 T in the darkness within the range from 5 to 300 K.

#### 4. Experimental results and discussion thereof

Fig. 5, *a* shows waveforms of electric field of terahertz pulses  $E_{\text{off}}(t)$  and  $E_{\text{on}}(t)$  obtained at a temperature of 90 K. The  $E_{\text{on}}(t)$  waveform of terahertz pulse is a maximum with positive and negative half-waves [27,28]. Maximum of the  $E_{\text{on}}(t)$  dependence corresponds to the dipole response of 2DEG, because it arises as a result of multiphoton absorption of femtosecond optical pulses in the QW. The superposition of multiple reflections of the terahertz pulse from the QW/QB interface was manifested on waveforms as positive half-waves. The phase shift by  $\pi$  due to the superposition of multiple reflections from the QW/QB interface can be related to negative half-waves in Fig. 5, *a*. The QB/QW and QW/QB interfaces are different from each other by the ratio of refractive indices of media.

Free carriers generated between the electrodes of PC2 by femtosecond pulses were accelerated by the electric field applied to the gap. As a result, a pulse of current arose,

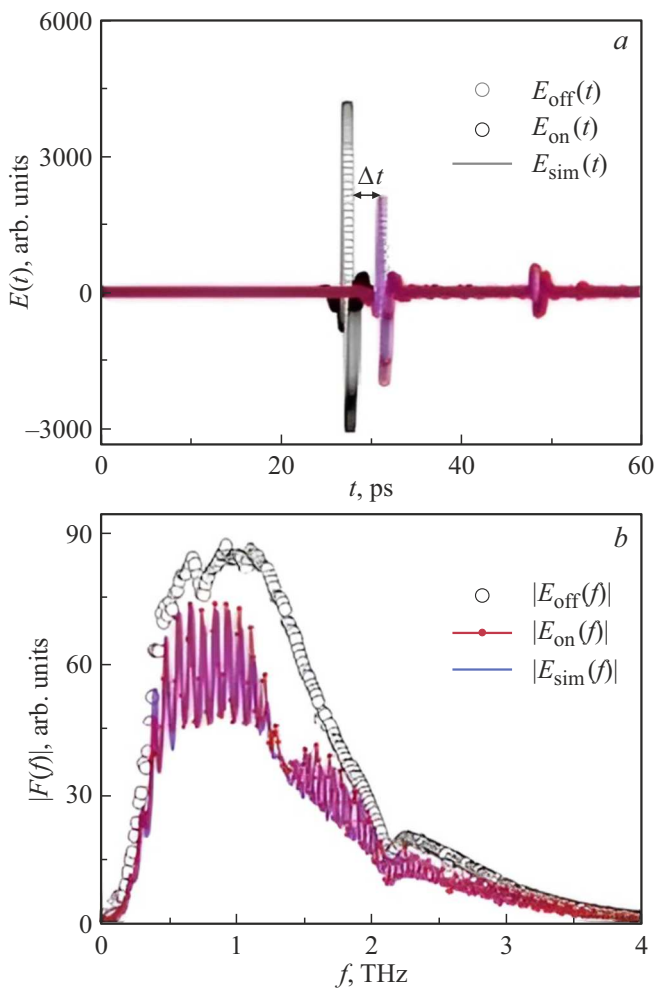


**Figure 5.** Waveforms of electric field of terahertz pulses (a) and result of fast Fourier transform application to the corresponding waveforms (b).

which was a source of terahertz radiation. Its waveform  $E_{\text{off}}(t)$  was recorded in accordance with the scheme shown in Fig. 2. The delay of the terahertz pulse recorded by the detector is due to the energy losses in layers of the heterostructure, as well as its partial reflection. The delay  $\Delta t$  equal to 2.3 ps is the relaxation time of the 2DEG pulse in three QWs of  $\text{In}_x\text{Ga}_{1-x}\text{N}/\text{GaN}$ . Reflections from the cryostat walls and from the substrate are related to the arising of the first and the second peaks of lower amplitude in Fig. 5, a.

Fig. 5, b shows frequency dependence of Fourier amplitude of terahertz pulses, as well as the modelled  $E_{\text{off}}(t)$  dependence. It can be seen, that there are three minima with resonance frequencies of 2D plasmon oscillations in the range from 1.5 to 3.5 THz. Results of modelling of terahertz pulses power and phase shift are shown in Fig. 6, a, b.

Oscillations of the  $P_{t1,t2}(f)$  and  $\Phi_{t1,t2}(f)$  functions within the frequency range from 1 to 3.5 THz, which are modulated by the Fabry-Perot bands are observed (Fig. 6, a). The „fringe“ effect on the  $P_{t1,t2}(f)$  and  $\Phi_{t1,t2}(f)$  spectra appears

due to reflection of the terahertz pulse from the substrate and its multiple interference in the plane-parallel layers of the  $\text{InGaN}/\text{AlGaIn}/\text{GaN}$  heterostructure. The Fabry-Perot bands on the  $P_{t2}(f)$  and  $\Phi_{t2}(f)$  frequency dependencies were suppressed by cutting signal channels before the first „echo“ on the time dependence (Fig. 5, a). Fig. 6, b shows frequency dependence of the terahertz pulse phase shift. It can be seen, that the phase shift near the plasmon resonances is a kink point of the  $\Phi_{t1,t2}(f)$  function, which corresponds to minima in the  $P_{t1,t2}(f)$  power frequency spectra. At temperatures over 170 K, features of the plasmon resonance were not resolved in the experiment. The first three frequencies are  $f_{g,1} = 1.7$  THz,  $f_{g,2} = 2.4$  THz,  $f_{g,3} = 3.3$  THz (Fig. 6, a).

In this study frequency dependencies of spectral power and phase shift of terahertz pulses were obtained in the temperature range from 90 to 170 K with a step of 20 K (Fig. 7).

The observed shift of 2D plasmon resonance frequency toward long-wave region (Fig. 7, a) from the value of

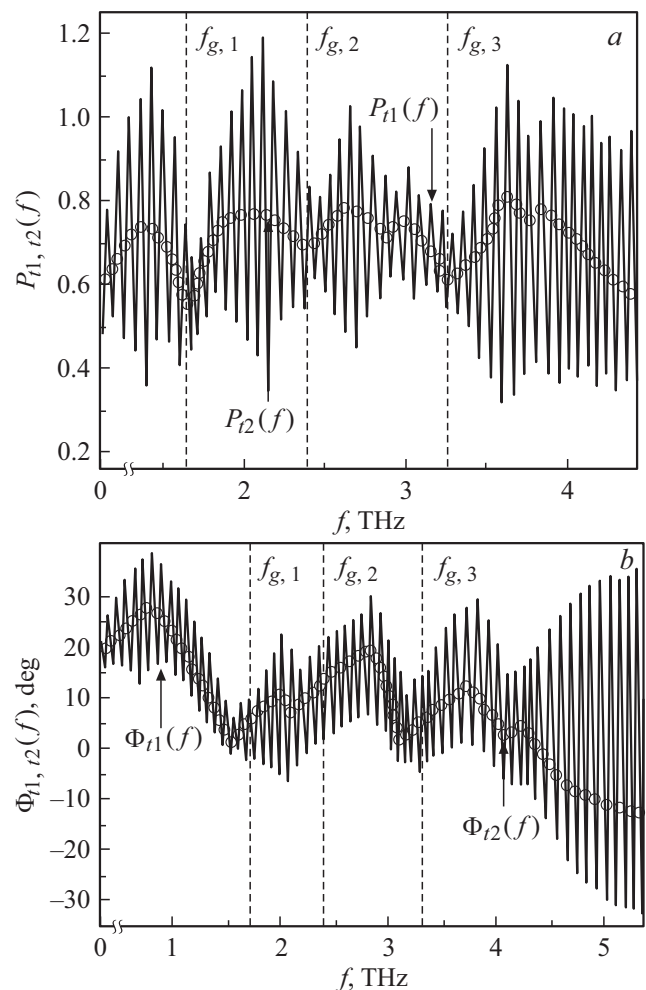


**Figure 6.** Frequency dependencies of power (a) and phase shift (b) of the terahertz radiation obtained under excitation by femtosecond laser pulses with a time window of  $t_1 = 130$  fs at a wavelength of 800 nm.

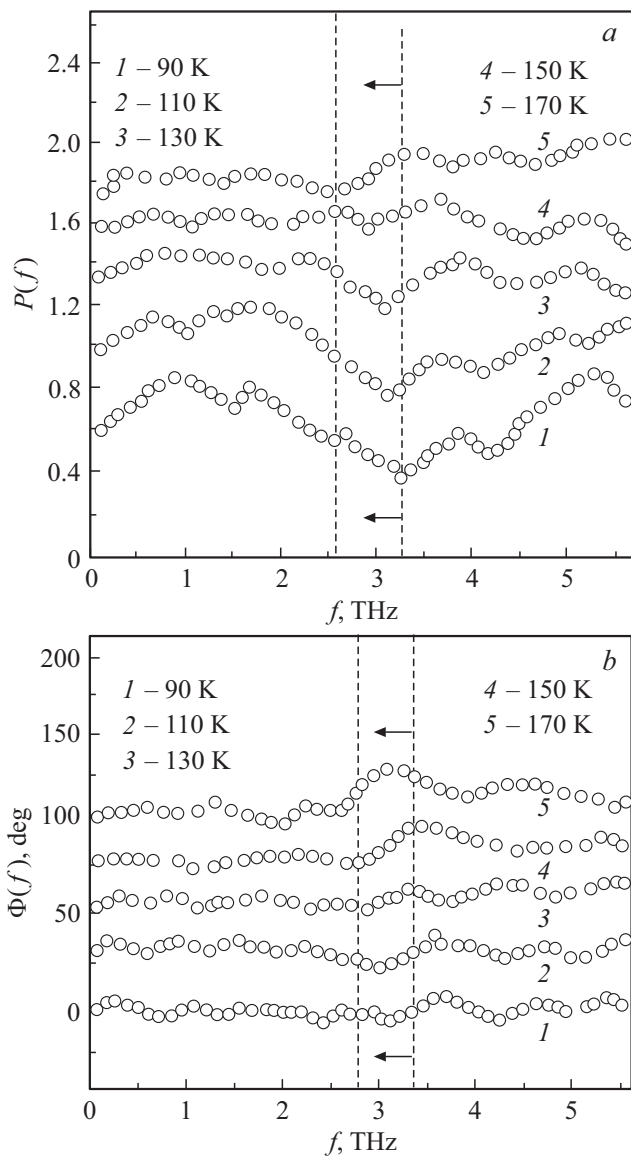


**Figure 7.** Power (a) and phase shift of terahertz pulses (b) obtained in the temperature range from 90 to 170 K with a step of 20 K. Dashed vertical lines show the position of frequencies of the plasmon resonances at sample temperatures of 90 and 170 K. Arrows mark the red shifting of the 2D plasmon resonance.

3.3 THz (at 90 K) to 2.5 THz (at 170 K) is identified in both  $P(f)$  and  $\Phi(f)$  spectra. The red shift of the 2D plasmon resonance may be related to the temperature dependence of the effective mass of the 2D electron gas. Table 2 demonstrates values of effective mass of 2DEG at temperatures of sample heating from 90 to 170 K calculated by formula (9). An increase in sample temperature results in broadening of the minimum of 2D plasmon resonance and suppression of its peak value (Fig. 7, a). At the same time an amplification of phase modulation is observed (Fig. 7, b). The amplitude kink is increased from  $3^\circ$  at 90 K to  $20^\circ$  at 170 K.

Then we have evaluated the total time of attenuation of plasmon oscillations in the 2DEG by frequency dependen-

**Table 2.** Temperature dependence of effective mass of 2DEG in three QWs of  $\text{In}_x\text{Ga}_{1-x}\text{N}/\text{GaN}$

$T, \text{K}$				
90	110	130	150	170
$0.43m$	$0.45m$	$0.45m$	$0.49m$	$0.56m$

**Table 3.** Temperature dependence of pulse relaxation time of 2DEG and total attenuation time

Decay time	$T, \text{K}$				
	90	110	130	150	170
$\tau, \text{ps}$	2.0	1.8	1.3	0.8	0.2
$\tau_{\text{gen}}, \text{ps}$	1.3	1.0	0.8	0.5	0.4

**Table 4.** Parameters of 2D electron gas as per data of frequencies of the two-dimensional plasmon resonances at a sample heating temperatures of 170 K

$N_{2\text{DEG}}, 10^{12} \text{cm}^{-2}$	$f_{g,1}, \text{THz}$	$\tau, \text{ps}$	$\langle m^* \rangle$	$\mu, 10^3 \text{cm}^2/\text{V} \cdot \text{s}$
2.17	2.6	0.2	$0.56m$	4.2

cies of the terahertz pulse spectral power on the basis of  $\tau_{\text{gen}} = 1/2\pi\Delta f_{g,n}$  relationship. To calculate the total time of attenuation  $\tau_{\text{gen}}$ , the value of  $\Delta f_{g,n}$  was determined as a width of minimum of the 2D plasmon resonance measured at its half-height (Fig. 6, a). Results of calculation of the total time of attenuation  $\tau_{\text{gen}}$  and the pulse relaxation time  $\tau$  of 2DEG in three QWs of  $\text{In}_x\text{Ga}_{1-x}\text{N}/\text{GaN}$  are presented in Table 3.

It can be seen from the data in Table 3, that the time of total attenuation demonstrates a less weak temperature dependence. In the low temperatures region the pulse relaxation time prevails over the time of total attenuation. In the region of higher temperatures values become comparable. This mismatch at low temperatures can be explained by the presence of other forms of energy loss.

1. Partial compensation for built-in piezoelectric field by external electric fields.

2. Losses of lattice defects.

3. Excitation of oblique plasmon waves.

Based on the pulse relaxation times and effective mass, the mobility of 2DEG in three QWs of  $\text{In}_x\text{Ga}_{1-x}\text{N}/\text{GaN}$  was calculated. Results of the calculation are presented in Table 4.

As can be seen from Fig. 8, a, the behavior of Hall concentration dependence on temperature is nonmonotonous. In the region of low temperatures ( $30 < T < 175 \text{K}$ ) the Hall concentration keeps its mean value about  $2.17 \cdot 10^{10} \text{cm}^{-2}$ . In the region of higher temperatures ( $T > 175 \text{K}$ )  $n_H(T)$  increases and achieves  $2.3 \cdot 10^{10} \text{cm}^{-2}$ .

**Table 5.** Hall mobility and concentration at low and high temperatures

30 K		170 K	
$n_H, 10^{12} \text{ cm}^{-2}$	$\mu_H, 10^3 \text{ cm}^2/\text{V} \cdot \text{s}$	$n_H, 10^{12} \text{ cm}^{-2}$	$\mu_H, 10^3 \text{ cm}^2/\text{V} \cdot \text{s}$
2.17	7	2.18	4.2

The temperature dependence of  $\mu_H(T)$  (Fig. 8, *b*) is typical for InGaN/AlGaIn/GaN heterostructures. The Hall mobility decreases with increase in temperature due to the increase in intensity of mechanisms of scattering on polar optical phonons at  $T > 85$  K.

The investigated sample of heterostructure with three QWs has a multilayer structure. It is also doped with a donor or acceptor impurity. Hence, the Hall mobility and concentration is mainly contributed by 2DEG. Values of  $n_H, \mu_H$  for two extreme temperature regions are presented in Table 5. The comparison of experimental data allowed us to identify differences and common patterns in behavior of relaxation times, mobility, and effective mass of 2DEG in heterostructures with three and five QWs. Based on the comparison between the obtained results and the data reported in [19], it can be claimed that in the case of multiphoton absorption of optical femtosecond pulses plasmon oscillations with typical resonance frequencies are generated in QWs of the active region of heterostructures. However, in the case of  $\text{In}_x\text{Ga}_{1-x}\text{N}/\text{GaN}$  heterostructures with three QWs the number of observed 2D plasmon resonances is equal to 3.

An increase in the number of QWs in the active layer is accompanied by a decrease in the number of observed resonances in power spectra of the terahertz radiation and a growth in the strength of the terahertz electric field [19]. If the change in speed of charge carriers over time is ignored, the electric field strength of the terahertz radiation can be evaluated by the formula of dipole radiation:

$$E_{\text{THz}} \sin \frac{\partial N}{\partial t} e \mu E_{\text{int}} \sin \vartheta, \quad (11)$$

where  $E_{\text{int}}$  is the strength of built-in electric field in the active region of heterostructure;  $\vartheta$  is the angle between the normal to the dipole oscillation direction and the direction of radiation;  $\partial N/\partial t$  is the change in photoinduced charge carriers concentration over time with a mobility of  $\mu$ .

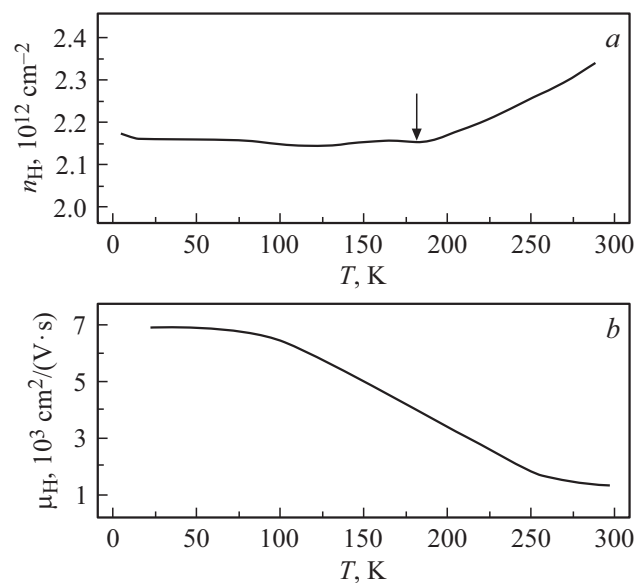
Built-in piezoelectric fields in the active region warp the valence band and the conduction band. The doping with donor and acceptor impurity results in lowering of the impurity Fermi level, i.e. promotes an increase in the difference between volumetric and surface Fermi levels. As a result, the valence band and the conduction band become even more warped, and the strength of built-in electric field in the heterostructure increases. Therefore, in the case of heterostructures with five QWs, which barriers are

doped with donor and acceptor impurity, the electric field strength of terahertz radiation according to formula (11) is higher. In order to understand why the number of observed resonances is lower, it is necessary to find out what is the distribution of the laser radiation energy, one part of which is dissipated in the layers of the heterostructure, and another part is spent for excitation of plasmon oscillations. For this purpose, it is necessary to analyze the relaxation time of 2DEG that increases with increase in the number of QWs from  $\sim 10^{-12}$  s (heterostructures with three QWs) to  $\sim 10^{-9}$  s (heterostructures with five QWs). This behavior pattern is explained by the presence of doping impurity in GaN barriers, which leads to an increase in strength of the built-in electric field that impedes the disorientation of oscillating dipoles excited by femtosecond laser pulses. Hence, the relaxation time of dipoles grows.

An increase in the number of QWS is accompanied with a decrease in phase modulation near the frequencies of plasmon resonances. For heterostructures with three QWs the amplitude kink is  $17^\circ$ , while for heterostructures with five QWs the temperature kink is  $14^\circ$ . In the process of studying the frequency dependencies of terahertz radiation phase shift it is found, that phase modulation exceeds tens of degrees (up to  $17^\circ$ ) near the frequencies of plasmon resonances.

In the temperature range from 30 to 170 K the Hall concentration is constant (Fig. 8, *a*). Hence, the effect of renormalization of the effective mass and the phase modulation is related not to temperature dependence of Hall concentration, but to the nonlinear dynamics of 2DEG.

It is worth to note, that studying the relaxation times of 2DEG in heterostructures can provide insight into the effective mechanisms of scattering and the contribution of each of them to the total channel of 2DEG relaxation. For

**Figure 8.** Temperature dependence of Hall concentration (*a*) and Hall mobility (*b*). The arrow indicates the beginning of growth of the experimental curve.

example, the relaxation times obtained for the case of five QWs ( $\sim 10^{-9}$  c) match well the theoretical data reported in [29], where the mechanism of piezoelectric scattering of 2DEG was investigated.

## 5. Conclusion

Thus, in this work the excitation of 2D plasmon resonances and recording of their frequencies by THz-TDs method are used to obtain values of pulse relaxation times, mobility, and effective mass of 2DEG in three QWs of  $\text{In}_x\text{Ga}_{1-x}\text{N}/\text{GaN}$ . It is found that 2DEG in three QWs of  $\text{In}_x\text{Ga}_{1-x}\text{N}/\text{GaN}$  is characterized by a pulse relaxation time of 0.2 ps, a mobility of  $4.2 \cdot 10^3 \text{ cm}^2/\text{V c}$ , and an effective mass of  $0.56m$  at a heating temperature of 170 K. The oscillating behavior of the output terahertz radiation power with minima in the frequency range from 1.5 to 3.5 THz is shown, which is related to the nonlinear dynamics of 2DEG in MQW of  $\text{In}_x\text{Ga}_{1-x}\text{N}/\text{GaN}$ . When studying the interactions between laser pulses with a length of 130 fs and a plasmon structure, frequency dependencies of power and phase shift of the terahertz radiation are obtained. The fast Fourier transform technique was applied to process terahertz spectra of emission. This allowed comparison of amplitudes and phases of Fourier-harmonic components. With the comparison of the frequency-dependent amplitudes and phases of the terahertz signal, the dynamics of the collective electron excitations in 2DEG has been studied. It is shown that with heating of the  $\text{InGaN}/\text{AlGaIn}/\text{GaN}$  heterostructure up to 170 K a red shift of the first plasmon resonance frequency from 3.3 to 2.5 THz is observed. In the course of work the dependence of effective mass versus temperature  $m^*(T)$  is obtained. In  $\text{In}_x\text{Ga}_{1-x}\text{N}/\text{GaN}$  heterostructures with three QWs the effective mass changes in the range from  $0.43m$  at 90 K to  $0.56m$  at 170 K, which is related to the renormalization of effective mass in the active region of the heterostructure.

The obtained values of mobility and pulse relaxation times of 2DEG in  $\text{In}_x\text{Ga}_{1-x}\text{N}/\text{GaN}$  heterostructures with three QWS can be used for optimization of process parameters of composite heterostructures growth and output radiation power of devices based on them. The performed studies are interesting for applications of physics, micro- and opto-electronics, where maximum possible mobility of 2DEG with the shortest possible life time is desirable.

## Conflict of interest

The authors declare that they have no conflict of interest.

## References

- [1] B. Richard, M. Schasfoort. Handbook of Surface Plasmon Resonance (2017). P. 555.
- [2] A. Ando, T. Kurose, V. Reymond, K. Kitano, H. Kitahara, K. Takano, M. Tani, M. Hangyo, S. Hamaguchi. J. Appl. Phys. **110**, 7 (2011).
- [3] S.P. Jamison, D.R. Jones, R.C. Issac, B. Ersfeld, D. Clark, D.A. Jaroszynski. J. Appl. Phys. **93**, 7, 4334 (2003).
- [4] C. Strothkämper, A. Bartelt, R. Eichberger, C. Kaufmann, T. Unold. Phys. Rev. B **89**, 11, 1 (2014).
- [5] A. Mendoza-Galvan, J. Gonzalez-Hernandez. J. Appl. Phys. **87**, 760 (2000).
- [6] M. Orío, D. Pantazis, F. Neese. Photosint. Res. **102**, 2, 443 (2009).
- [7] G. Sun, R. Chen, Y. J. Ding. IEEE J. Sel. Top. Quantum Electron. **19** (2013).
- [8] I. Prudaev, S. Sarkisov, O. Tolbanov, A. Kosobutsky. Phys. Status Solidi B **252**, 5, 946 (2015).
- [9] W. Rehman, R.L. Milot, G.E. Eperon, C. Wehrenfennig, J.L. Boland, H.J. Snaith, M.B. Johnston, L.M. Herz. Adv. Mater. **27**, 48 (2015).
- [10] G.R. Yettapu, D. Talukdar, S. Sarkar, A. Swarnkar, A. Nag, P. Ghosh, P. Mandal. Nano lett. **16**, 8 (2016).
- [11] A.M. Ulatowski, L.M. Herz, M.B. Johnston. J. Infrared, Millimeter, Terahertz Waves **41**, 12, 1431 (2020).
- [12] P.J.S. van Capel, D. Turchinovich, H.P. Porte, S. Lahmann, U. Rossow, A. Hangleiter, J.I. Dijkhuis. Phys. Rev. B **84** (2011).
- [13] G. Sun, G. Xu, Y. J. Ding. IEEE J. Sel. Top. Quantum Electron. **17**, 48 (2011).
- [14] H.P. Porte, D. Turchinovich, D.G. Cooke, P.U. Jepsen. J. Phys.: Conf. Ser. **193**, 012084 (2009).
- [15] M.L. Badgutdinov, A.E. Yunovich, FTP **42**, 4, 438 (2008) (in Russian).
- [16] V.I. Oleshko, S.G. Gorina, Uch. zap. fiz. fak. **5**, 155501, 1 (2015) (in Russian).
- [17] V.G. Mokerov, A.L. Kuznetsov, Yu.V. Fedorov, Ye.N. Yenyushkina, A.S. Bugayev, A.Yu. Pavlov, D.L. Gnatyuk, A.V. Zuyev, R.R. Galiyev, Ye.N. Ovcharenko, Ye.N. Sveshnikov, A.F. Tsal'sul'nikov, V.M. Ustinov, FTP **43**, 4, 561 (2009) (in Russian).
- [18] J.M. Hensley, J. Montoya, M.G. Allen, J. Xu, L. Mahler, A. Tredicucci, H.E. Beere, D.A. Ritchie. Opt. Express **22**, 17, 20476 (2009).
- [19] Ye.R. Burmistrov, L.P. Avakyants, FTP **55**, 11, 1059 (2021) (in Russian).
- [20] L.P. Avakyants, A.E. Aslanyan, P.Y. Bokov, A.V. Chervyakov, K.Y. Polozhentsev. Solid State Elektron. **130**, 4, 45 (2017).
- [21] G. Franssen, P. Perlin, T. Suski. Phys. Rev. B **69**, 4 (2004).
- [22] L.P. Avakyants, P.Yu. Bokov, T.P. Kolmakova, A.V. Chervyakov, FTP **38**, 12 (2004) (in Russian).
- [23] S.L. Chuang, S. Schmitt-Rink, B.I. Greene, P.N. Saeta, A.F.J. Levi. Phys. Rev. Lett. **68**, 1, 102 (1992).
- [24] Z. Chang. Phys. Rev. A **70**, 4, 043802-1 (2004).
- [25] P. Schley, R. Goldhahn, G. Gobsch, M. Feneberg, K. Thonke, X. Wang, A. Yoshikawa. Phys. Status Solidi B **246**, 6, 8 (2009).
- [26] S.J. Allen, D.C. Tsui, R.A. Logan. Phys. Rev. Lett. **38**, 980 (1977).
- [27] V.L. Malevich, G.V. Sinitsyn, N.N. Rozanov, Optika i spektroskopiya **127**, 4, 667 (2019) (in Russian).
- [28] R.R. Pelá, C. Cactano, M. Marques, L.G. Ferreira, J. Furthmüller, L.K. Teles. Appl. Phys. Lett. **98**, 15, 14 (2011).
- [29] E.R. Burmistrov, L.P. Avakyants. Izv. vuzov. Fizika **64**, 5, 9 (2021) (in Russian).

Translated by Ego Translating